A study on a lobed jet mixing flow by using stereoscopic particle image velocimetry technique

Cite as: Physics of Fluids **13**, 3425 (2001); https://doi.org/10.1063/1.1409537
Submitted: 18 September 2000 • Accepted: 31 July 2001 • Published Online: 15 October 2001

Hui Hu, Tetsuo Saga, Toshio Kobayashi, et al.

A study on a lobed jet mixing flow by using stereoscopic particle image velocimetry technique

Hui Hu,[a] Tetsuo Saga, Toshio Kobayashi, and Nobuyuki Taniguchi
Institute of Industrial Science, University of Tokyo, 4-6-1 Komaba, Meguro-ku, Tokyo 153-8505, Japan

(Received 18 September 2000; accepted 31 July 2001)

In a continuing effort to study the mixing enhancement by large-scale streamwise vortices generated by a lobed nozzle, a high-resolution stereoscopic particle image velocimetry (PIV) system was used in the present study to conduct three-dimensional measurements of air jet flows exhausted from a lobed nozzle and a conventional circular nozzle. The three-dimensional instantaneous and ensemble-averaged velocity fields, instantaneous and ensemble-averaged streamwise vorticity distributions and turbulent kinetic energy distributions were used to analyze the characteristics of the mixing process in the lobed jet flow compared with conventional circular jet flow. The existence of large-scale streamwise vortices in the lobed jet mixing flow is revealed clearly from the stereoscopic PIV measurement results. The instantaneous streamwise vorticity distributions revealed that the large-scale streamwise vortices generated by the corrugated trailing edge of the lobed nozzle break into smaller, but not weaker streamwise vortices gradually as they travel downstream. This is the proposed reason why a lobed nozzle would enhance both large-scale mixing and small-scale mixing reported by other researchers. The overall effect of the lobed nozzle on the mixing process in the lobed jet mixing flow was evaluated by analyzing the ensemble-averaged streamwise vorticity distributions. It was found that ensemble-averaged streamwise vortices in the lobed jet mixing flow grew up and expanded radially over the first diameter of the test nozzle, then began to break down into smaller and weaker vortices further downstream. The averaged turbulent kinetic energy profile indicated that most of the intensive mixing between the core jet flow and ambient flow, due to the special geometry of the lobed nozzle, occurred within the first two diameters of the lobed nozzle, which corresponds to the upstream region where the ensemble-averaged streamwise vortices break down. [DOI: 10.1063/1.1409537]

INTRODUCTION

The physics of the mixing process is of considerable interest from both fundamental and practical points of view. It has been widely suggested that the mixing process is intimately connected with the transient of turbulence. In engineering flows, the mixing process governs the mixing rate in combustion chambers, jet noise level of airplanes and vehicles, and the spread of pollutants at industrial sites. A critical technical problem to be solved in many of these applications is mixing enhancement of a jet flow with ambient flows. How quickly and how well a jet flow can be mixed with ambient flows will have a major influence on combustion efficiency, heat release rate, pollutant formation, jet noise suppression and size reduction of such functional devices.

The streamwise vortices generated in a jet flow, in addition to the azimuthal (or ring type) vortices, have been found to mix fluid streams even more efficiently. As pointed out in the investigations of Zaman,[1] both the azimuthal and streamwise vorticities are of equal importance to jet mixing process and they are not independent of each other. The distortion of azimuthal vortex structure may lead to streamwise vortices under certain conditions. The streamwise vortices in jet mixing flows can be generated by many methods. For example, a lobed nozzle used to generate large-scale streamwise vortices in a jet flow has been considered to be a promising method for jet mixing enhancement.

A lobed nozzle, which consists of a splitter plate with corrugated trailing edge, has been given great attention by many researchers in recent years. It has also been applied widely in turbofan engine exhausts and ejectors. For example, for some commercial aero-engines, such as JT8D-217C, CFM56-5C, and RB211-524G/H (which are widely used on Boeing and Airbus airplanes), lobed nozzles/mixers has been used to reduce take-off jet noise and specific fuel consumption (SFC).[2,3] In order to reduce the infrared radiation signals of military aircraft to improve their survivability, lobed nozzles/mixers have also been used to enhance the mixing process of the high temperature and high-speed gas plume from air-engine with ambient cold air.[4,5] These military aircraft include the military helicopter ''Tiger'' developed by Germany and France, the American helicopter RAH-66 ''Comanche'' and stealth Fighter F-117. More recently, lobed nozzles have also emerged as an attractive approach for enhancing mixing between fuel and air in com-

[a]Author to whom correspondence should be addressed. Present address: Turbulent Mixing and Unsteady Aerodynamics Laboratory, A22, Research Complex Engineering, Michigan State University, East Lansing, Michigan 48824; electronic mail: huhui@egr.msu.edu

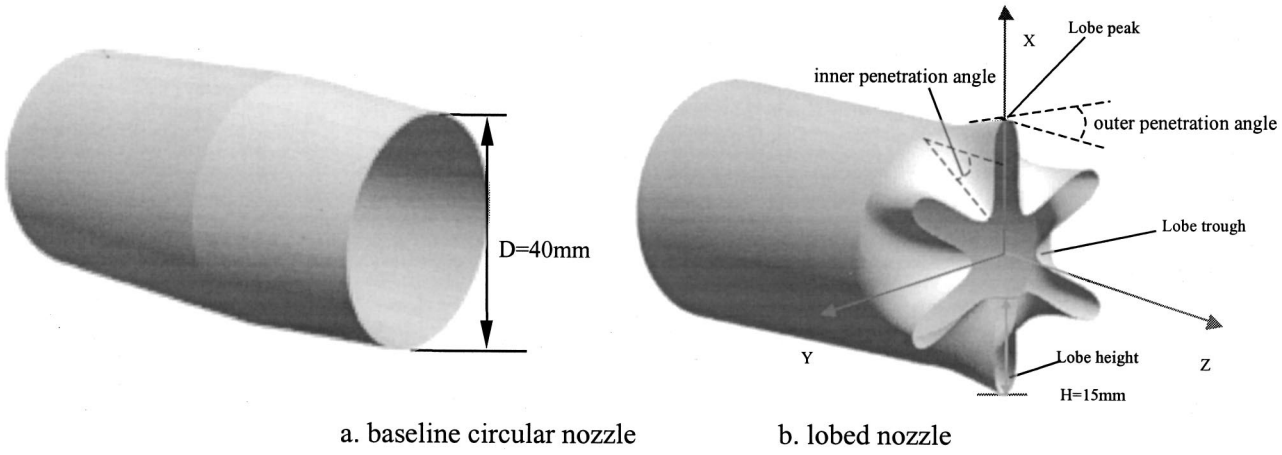

FIG. 1. The test nozzles.

bustion chambers to improve the efficiency of combustion and reduce the formation of pollutants.[6]

Most early studies of lobed nozzles/mixers were concentrated on optimizing the geometry design of lobed nozzles/mixers for bulk mixing enhancement. The findings of those studies include that lobes with parallel sides can achieve higher mixing performance compared with sinusoidal shaped lobes[7] scalloping the lobes aids in mixing.[8] The lobe penetration in the fluid streams has the most significant effect on mixing effectiveness as long as the flow does not separate.[9]

Paterson[10] is considered to be the first to research the fluid dynamical mechanism of the mixing process downstream of a lobed nozzle/mixer. Based on the detailed pressure and temperature data as well as three-dimensional laser Doppler velocimetry (LDV) measurement results of the velocity field, Paterson[10] found that the lobed nozzle could produce streamwise vortices with length scale on the order of the nozzle radius. Horseshoe vortices with smaller scale were also found to exist at the lobe troughs. The contribution of these vortices to the overall mixing process was not clear, but the secondary flows (streamwise vortices) were expected to be dominant because of their much greater size.

Much of the later work on lobed nozzle/mixer concentrated on discovering the underlying physics of the lobed mixing process by using two-dimensional lobed mixer, which is essentially a corrugated plate. Werle *et al.*[11] suggested that the large-scale streamwise vortex formation process was an inviscid one. The mixing process in the lobed mixing flow was suggested to take place in three basic steps: (1) The vortices form, (2) intensify and then (3) rapidly break down into smaller turbulence. So the lobed mixer was thought to act as a fluid stirrer initially to mix the flow, until the vortices break down to produce small scale mixing.

Eckerle *et al.*[12] used a two-dimensional LDV system to study the mixing process downstream of a planar lobed mixer at two velocity ratios of the two mixing streams. They reported that the breakdown of the large-scale streamwise vortices and the accompanying increase in turbulent mixing are important parts of the mixing process. They also found that the vortex breakdown occurs further upstream for the velocity ratio 2:1 case rather than for 1:1 case.

Elliott *et al.*[13] found that both the streamwise vortices shed from lobed trailing edge and the increased initial interfacial area associated with the lobe geometry are also significant for increasing mixing compared to that occurring within conventional flat plate splitter. At velocity ratio close to 1.0, the increased mixing is due mainly to the increased contact area, whereas the streamwise vortices have a larger role at a velocity ratio of 2.0, and its importance rises as the velocity ratio increases.

The study by McCormick *et al.*[14] revealed more details about the flow patterns downstream of a planar lobed mixer. Based on the pulsed-laser sheet flow visualization with smoke and three-dimensional velocity measurements with hot film anemometer (HFA), they suggested that the interaction of Kelvin–Helmholtz (azimuthal) vortices with the streamwise vortices produce the high levels of mixing. The streamwise vortices deform the Kelvin–Helmholtz (azimuthal) vortices into pinch-off structures and increase the stirring effect in the mixing flow. These result in the creation of intense small-scale turbulence and mixing.

Ukeiley *et al.*[15,16] and Glauser *et al.*[17] measured a planar lobed mixer flow field by using a rake of hot wires. Based on the proper orthogonal decomposition (POD) analysis and pseudo-flow visualization (PFV) of the data from the hot wire rake, they suggested that the turbulence dominated mixing in the lobed mixer flow field is due to the collapse of the pinch-off shear layer. The collapse of the shear layer onto itself, which occurred 3 to 6 times of the lobe height downstream, induced a burst of energy characterized by a region or pocket of high turbulence intensity.

In the paper of Belovich and Samimy,[18] the results of those previous studies were summarized by stating that the mixing process in a lobed nozzle/mixer is controlled by three primary elements. The first is the streamwise vortices generated due to the lobed shape. The second is the increase in interfacial area between the two flows due to the special geometry of lobed structures, and the third is the Brown–Roshko-type structures occurring in any shear layer due to the Kelvin–Helmholtz instabilities.

Although many important results were obtained in those previous studies, much work is still needed in order to un-

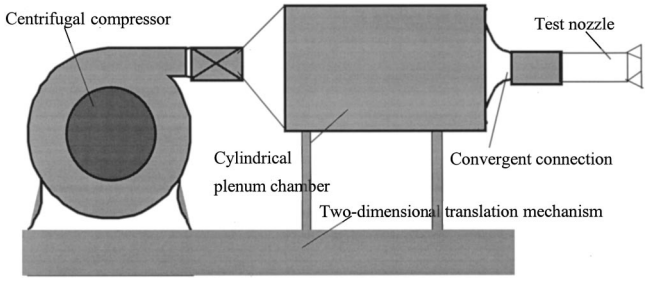

FIG. 2. The air jet experimental rig.

derstand the flow dynamics of the mixing enhancement using lobed nozzles. Previous studies have revealed the existence of unsteady vortical and turbulent structures in lobed mixing flows by qualitative flow visualization. However, quantitative information about the evolution of these unsteady vortical and turbulent structures is far more limited. The experimental techniques used in most previous studies were Pitot probe, laser Doppler velocimetry (LDV) or hot film anemometer (HFA). It is very hard to detail the unsteady vortical and turbulent structures in lobed mixing flows instantaneously and globally due to the limitation of these experimental techniques.

With the rapid development of modern optical techniques and digital image processing techniques, whole-field optical diagnostic technique like particle image velocimetry (PIV) is assuming an ever-expanding role in the diagnostic probing of fluid mechanics. The advances of PIV technique in recent decades have lead it to become a matured technique for whole-field measurements of fluid flow. In an earlier work of the authors,[19] both planar laser induced fluorescence (LIF) and particle image velocimetry (PIV) techniques were used to study lobed jet mixing flows in a water channel. By using directly perceived LIF flow visualization images and quantitative velocity, vorticity, and turbulence intensity distributions of PIV measurement results, the evolution and interaction characteristics of the various vortical and turbulent structures in the lobed jet mixing flows were discussed.

The PIV measurement results reported in the earlier work of the authors[19] was obtained by using a conventional two-dimensional PIV system in a water channel. It is well known that a conventional PIV system is only capable of recording the projection of velocity into the plane of the laser sheet. That means the out-of-plane velocity component is lost while the in-plane components may be affected by an unrecoverable error due to the perspective transformation.[20] For the highly three-dimensional flow fields like lobed jet mixing flows, the two-dimensional measurement results may not be able to reveal their three-dimensional features successfully. A high-resolution stereoscopic PIV system is used in the present study to measure the near flow field of a lobed jet mixing flow in order to reveal the three-dimensional features of the lobed jet mixing flow more clearly. The characteristics of the mixing process in a lobed jet mixing flow compared with a conventional circular jet flow will be discussed based on the three-dimensional measurement results of the stereoscopic PIV system.

EXPERIMENTAL SETUP AND THE STEREOSCOPIC PIV SYSTEM

Figure 1 shows the two test nozzles used in the present study; namely a baseline circular nozzle and a lobed nozzle with six lobes. The width of each lobe is 6 mm and the height of lobes is 15 mm ($H=15$ mm). The inner and outer penetration angles of the lobed structures are $\theta_{in}=22°$ and $\theta_{out}=14°$, respectively. The equivalent diameters of the two nozzles are designed to be the same, i.e., $D=40$ mm.

Figure 2 shows the air jet experimental rig used in the present study. A centrifugal compressor was used to supply air jet flows. A cylindrical plenum chamber with honeycomb was used to settle the airflow. Through a convergent connection (contraction ratio is about 50:1), the airflow is exhausted from the test nozzles. The whole jet supply rig was installed on a two-dimensional translation mechanism, which can be used to change the position of the test nozzles.

The velocity of the air jet exhausting from the test nozzle can be adjusted. In the present study, the core jet velocity (U_0) was set at about 20 m/s. The Reynolds number of the jet flow, based on the nozzle diameter (D) and the core jet velocity is about 60 000.

The air jet flows were seeded with small DEHS (di-2-

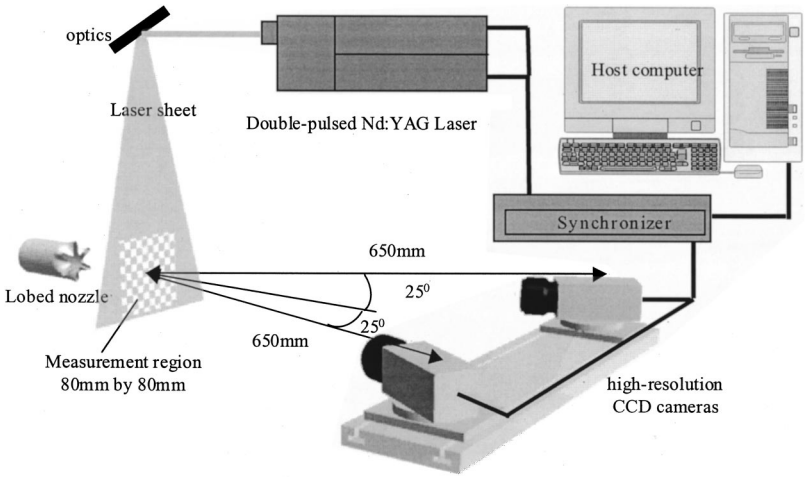

FIG. 3. The schematic of the stereoscopic PIV system.

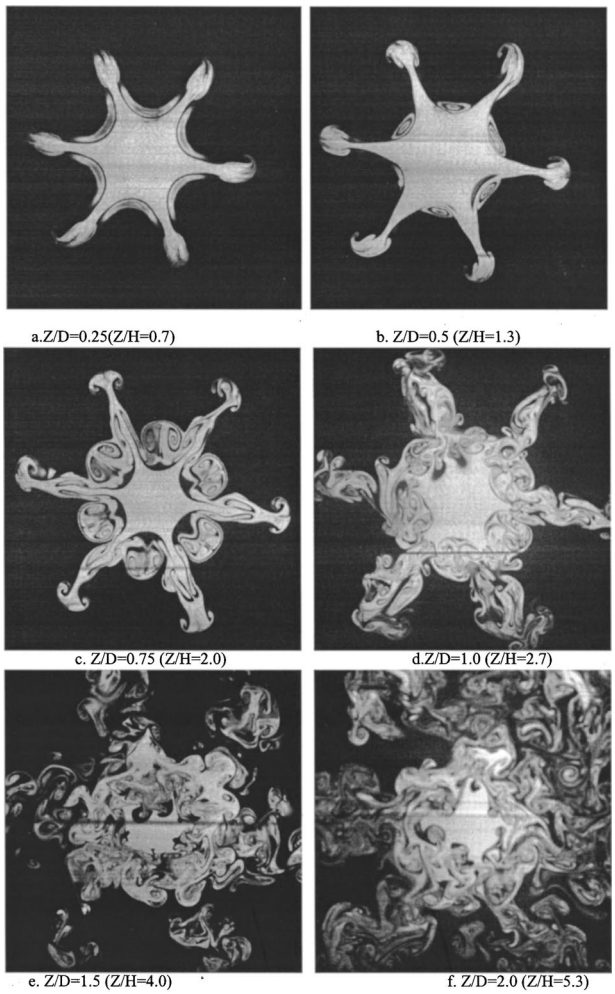

FIG. 4. PLIF flow visualization results of the lobed jet mixing flow in water chanal (Re=3000).

ethlhexyl-sebact) droplets generated by a seeding generator. The seeding generator is composed of an air compressor and several modified Laskin nozzles.[21] The diameter of the DEHS droplets used in the present study is about 1 to 5 μ m. The DEHS droplets out of the seeding generator were divided into two streams; one is used to seed the core jet flow and another for the ambient air seeding.

Figure 3 shows the schematic of the stereoscopic PIV system used in the present study. The objective jet mixing flows were illuminated by a double-pulsed Nd:YAG laser set (New Wave 50 mJ/Pulse) with the laser sheet thickness being about 2 mm. The double-pulsed Nd:YAG laser set can supply the pulsed laser (pulsed illumination duration 6 ns) at the frequency of 15 Hz. Two high-resolution (1 K by 1 K) cross-correlation CCD cameras (TSI PIVCAM10-30) were used to do stereoscopic PIV image recording. The two CCD cameras were arranged in an angular displacement configuration to maximize the measurement window size. In order to have the measurement field focused on the image planes perfectly, tilt-axis mounts were installed between the camera bodies and lenses, the lenses and camera bodies were adjusted to satisfy the Scheimpflug condition.[22] In the present study, the distance between the illuminating laser sheet and image recording plane of the CCD camera is about 650 mm, and the angle between the view axis of the two cameras is about 50°. For such arrangement, the size of the overlapped view of the two image recording cameras for stereoscopic PIV measurement is about 80 mm by 80 mm.

The CCD cameras and double-pulsed Nd:YAG lasers were connected to a workstation (host computer) via a synchronizer (TSI LaserPulse synchronizer), which controlled the timing of the laser sheet illumination and the CCD camera data acquisition. In the present study, the time interval between the two pulsed illuminations was set as 30 μs. The host computer is composed of two high-speed CPU (450 mHz, Pentium III CPU), colossal image memory and hard disk (1 GB RAM, Hard Disk 100 GB). It can acquire continuous stereoscopic PIV image pairs up to 250 frames every time at the framing frequency of 15 Hz.

Since the angular displacement method was used in the present study to do stereoscopic image recording, the magnification factors between the image planes and object plane are variable due to the perspective distortion. In order to determine the local magnification factors, an *in situ* calibration procedure was conducted in the present study to obtain the mapping functions between the image planes and object plane.

Following the work of Soloff *et al.*,[23] the *in situ* calibration procedure involved the acquisition of several images of a calibration target plate, say a Cartesian grid of small dots, across the thickness of the laser sheets. Then, these images were used to determine the magnification matrices of the image recording cameras. This method, which determines the mapping functions between the image planes and object planes mathematically,[24] therefore, takes into account the various distorting influences between test section and the CCD arrays of the image recording cameras. With the mapping functions determined by this method, the stereoscopic displacement fields obtained during the experiment are readily recombined into three-dimensional velocity vector fields.[25]

To accomplish the *in situ* calibration in the present study, a target plate (100 mm by 100 mm) with 100 μm diameter dots spaced at interval of 2.5 mm was used. The front surface of the target plate was aligned with the center of the laser sheet and then calibration images were captured at three locations across the depth of the laser sheets. The space interval between these locations was 0.5 mm for the present study.

The mapping function used in the present study was taken to be a multidimensional polynomial, which is fourth order for the directions (X and Y directions) paralleling the laser sheet plane and second order for the direction (Z direction) normal to the laser sheet plane. The coefficients of the multidimensional polynomial were determined from the calibration images by using least-square method.[26]

The two-dimensional particle image displacements in every image plane were calculated separately by using a Hierarchical Recursive–PIV (HR–PIV) software developed ''in-house.'' The hierarchical recursive–PIV software is based on hierarchical recursive processes of conventional spatial correlation operation with offsetting of the displace-

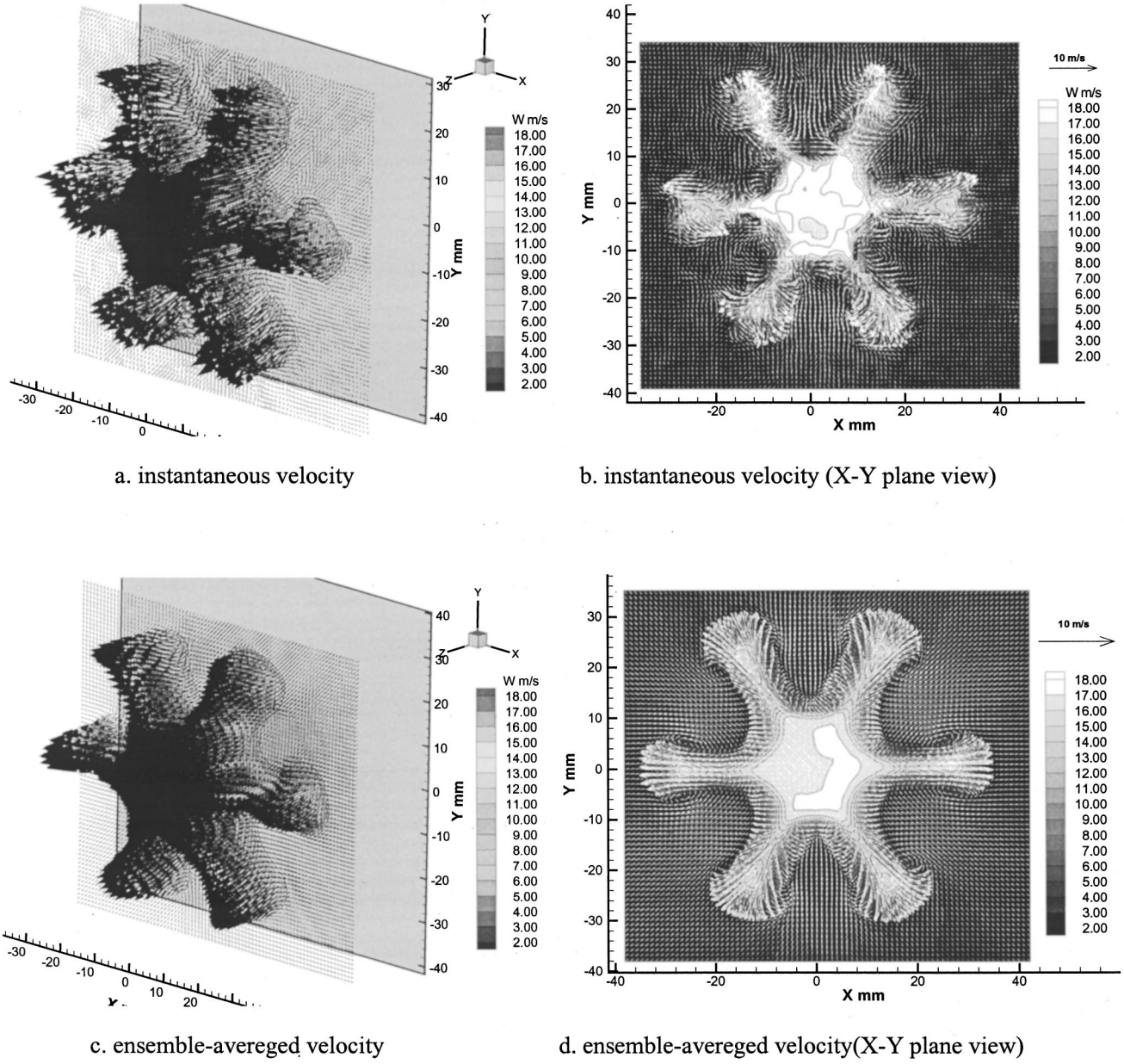

FIG. 5. Stereoscopic PIV measurement results in the $Z/D=0.5$ ($Z/H=1.33$) cross plane of the lobed jet mixing flow.

ment estimated by the former iteration step and hierarchical reduction of the interrogation window size and search distance in the next iteration step.[27] Multiple-correlation validation technique[28] and sub-pixel interpolation treatment[29] are also incorporated in the software. Compared with conventional cross-correlation based PIV image processing methods, the hierarchical recursive–PIV method has advantages in the spurious vector suppression and spatial resolution improvement of PIV result.

Finally, by using the mapping functions obtained by the *in situ* calibration procedure described previously and the two-dimensional displacements in the two stereoscopic image planes, the three components of the velocity vectors in the illuminating laser sheet plane were reconstructed.

The position of the illuminating laser sheet and image recording CCD cameras were fixed during the experiment. The distance changing between the exit of the test nozzles and the illuminating laser sheet was achieved by operating the two-dimensional translation mechanism (Fig. 2) to change the position of the air jet experimental rig. Such arrangement can insure that all the stereoscopic PIV measurements at different cross planes of the jet mixing flows are conducted while doing the *in situ* calibration procedure only once.

In order to evaluate the measurement results of the present stereoscopic PIV system, a LDV system was used to do simultaneous measurement of the lobed jet mixing flow. The stereoscopic PIV measurement results were compared with the LDV results. It was found that the difference between the measurement results of the present stereoscopic PIV system and LDV data is less than 2%. Further details about the present stereoscopic PIV system, the *in situ* calibration procedure and the comparison of the stereoscopic PIV and LDV measurement results can be found in Ref. 30.

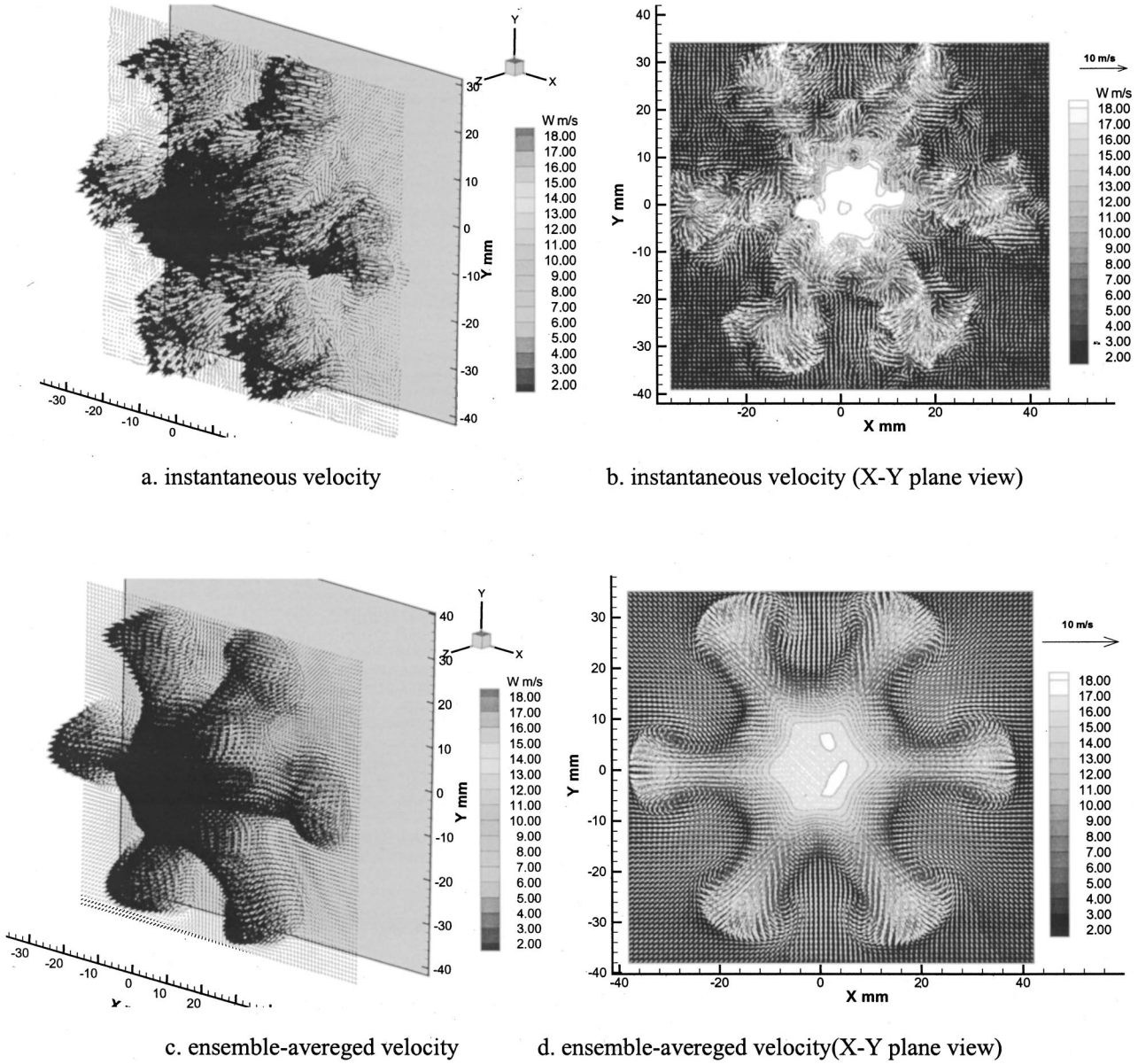

FIG. 6. Stereoscopic PIV measurement results in the $Z/D=1.0$ ($Z/H=2.67$) cross plane of the lobed jet mixing flow.

EXPERIMENTAL RESULTS AND DISCUSSIONS

The large-scale streamwise vortices generated by the lobed nozzle and azimuthal Kelvin–Helmholtz vortices are suggested to pay important roles in the mixing process of core jet flow with ambient flow. Figure 4, taken form Ref. 19, illustrates the evolutions and interactions of these vortices qualitatively. The pictures are planar LIF flow visualization images of a lobed jet mixing flow exhausted from the same lobed nozzle used in the present study. Downstream of the lobed nozzle trailing edge ($Z/D=0.25$, $Z/H=0.67$), the existence of the streamwise vortices in the form of six petal ''mushrooms'' at the lobe peaks can be seen clearly. The azimuthal Kelvin–Helmholtz vortices rolled up earlier at the lobe troughs were found to be six ''crescents'' at this cross section. As the streamwise distance increased to $Z/D=0.5$ ($Z/H=1.33$), the ''mushrooms'' at the lobe peak grew up, which indicated the intensification of the streamwise vortices generated by the lobed nozzle. Further downstream cross plane of $Z/D=0.75$ ($Z/H=2.0$), the streamwise vortices generated by the lobed nozzle in the form of ''mushroom'' structures continue intensification. Six new counter-rotating streamwise vortex pairs can be found at lobe troughs, which are called horseshoe vortex structures by Paterson.[10] In the cross plane of $Z/D=1.0$ ($Z/H=2.67$), some small-scale vortical and turbulent structures were found to appear in the flow. The interaction between the streamwise vortices and azimuthal Kelvin–Helmholtz vortices made adjacent ''mushrooms'' merge with each other, which may indicate that the streamwise vortices deform the azimuthal Kelvin–Helmholtz vortical tube into pinch-off structures as suggested by McCormick and Bennett.[14] In $Z/D=1.5$ ($Z/H=4.0$) and $Z/D=2.0$ ($Z/H=5.33$) downstream cross-planes, the ''mushroom'' shape structures almost disappeared and the flow field was filled with small-scale turbulent and vortical structures.

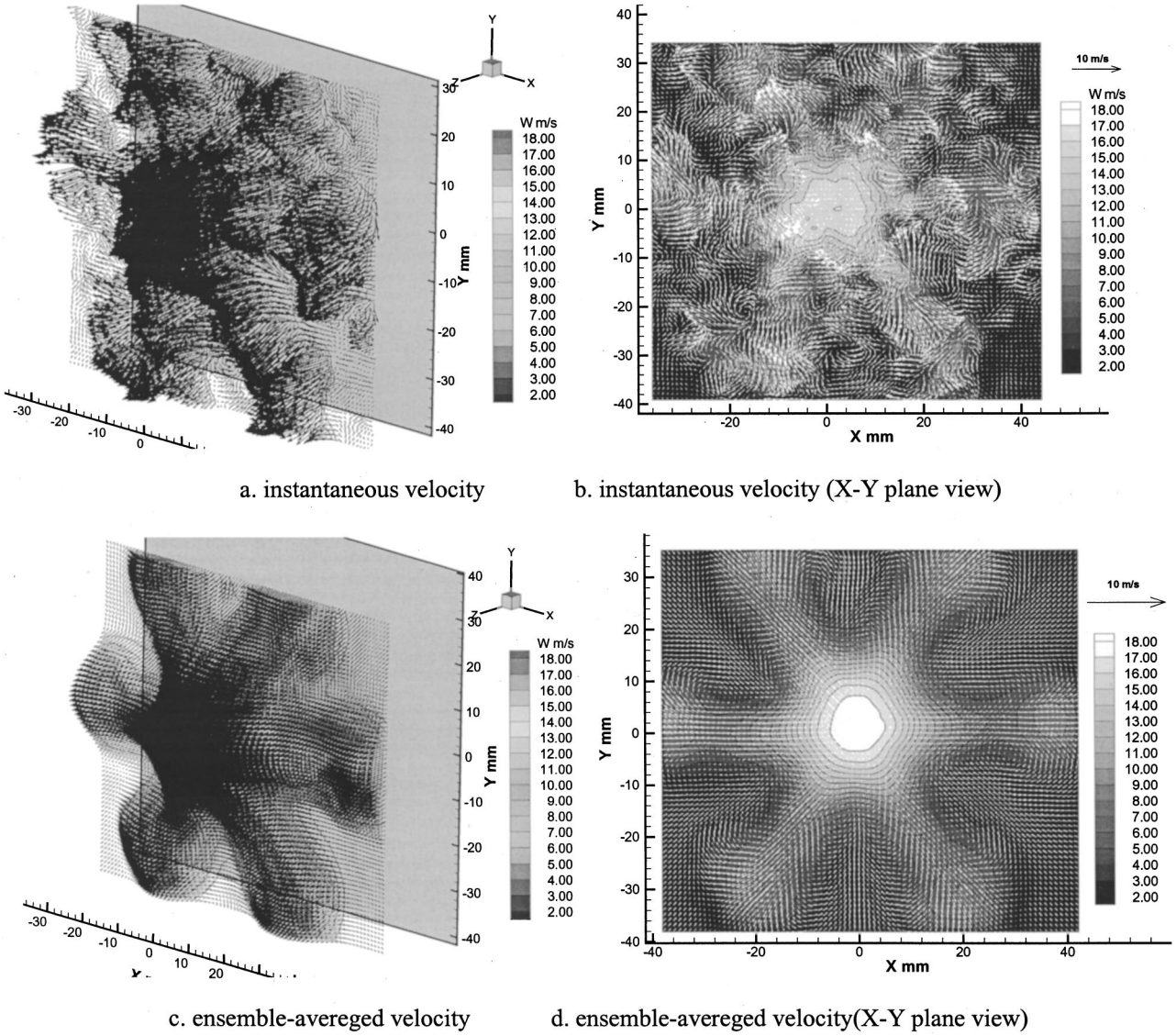

FIG. 7. Stereoscopic PIV measurement results in the $Z/D=2.0$ ($Z/H=5.33$) cross plane of the lobed jet mixing flow.

The stereoscopic PIV measurement results of the present study will give quantitative information about the evolution and interaction of these vortices.

The velocity distributions in the lobed jet mixing flow and circular jet flow

Figures 5–8 shows the stereoscopic PIV measurement results at four typical cross-planes of the lobed jet mixing flow, which include instantaneous velocity fields and ensemble-averaged velocity fields. In the present study, the ensemble-averaged velocity fields were calculated using 400 instantaneous stereoscopic PIV measurement results. The projections of the three-dimensional velocity vector in the cross planes ($X-Y$ plane views) were also given in the figures in order to reveal the cross stream (streamwise vortices) in the lobed mixing flow more clearly.

In the $Z/D=0.5$ ($Z/H=1.33$) cross plane, the lobed jet flow was found to be in the same geometry as the lobed nozzle trailing edge. The ''signature'' of the lobe nozzle in the form of ''six-lobe structure'' can be seen clearly from both the instantaneous and ensemble-averaged velocity fields (Fig. 5). Seven high-speed peaks can be seen from the ensemble-averaged velocity field, which represent the six lobes and the central core. From the $X-Y$ plane view of the ensemble-averaged velocity field shown in Fig. 5(d), a strong cross stream was found to exist in the lobe jet mixing flow. The core jet flow expanded outward in the lobe regions and ambient flow injected inward in the lobe trough regions. Both the core jet flow and ambient flow are generally following the inward and outward contours of the lobed nozzle, which results in the large-scale streamwise vortices seen in the lobed jet mixing flow. The maximum cross stream ensemble-averaged velocity in the $X-Y$ plane is found to be about 4.7 m/s at this cross plane. This value is found to be almost the same value as $U_0 \cdot \sin(\theta_{\text{out}})$, where U_0 is the core jet velocity at nozzle exit and θ_{out} is the outer penetration angle of the lobes.

Figure 6 shows the stereoscopic PIV measurement results in the $Z/D=1.0$ ($Z/H=2.67$) cross plane of the lobed jet mixing flow. The instantaneous velocity field was found

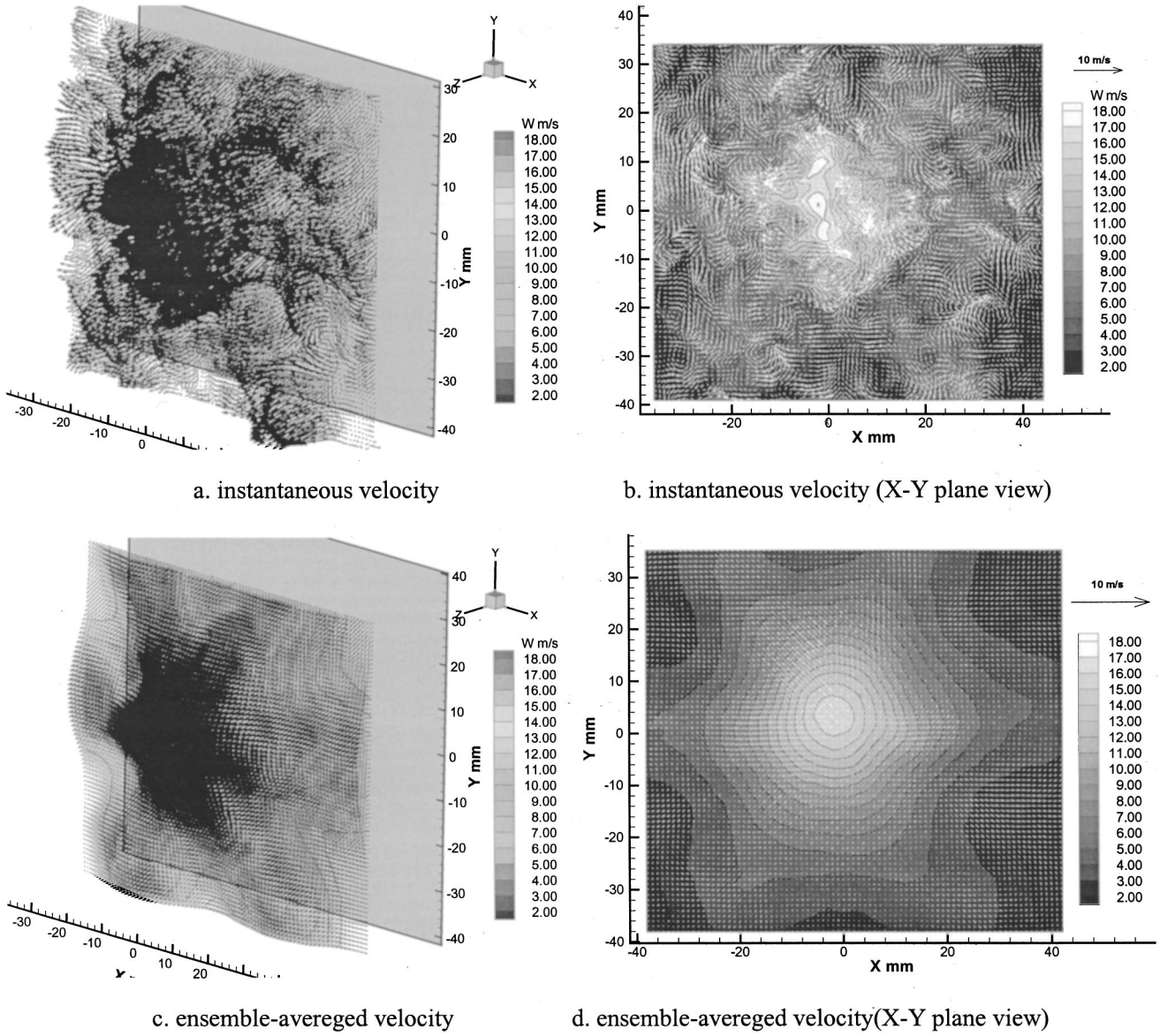

FIG. 8. Stereoscopic PIV measurement results in the $Z/D=3.0$ ($Z/H=8.0$) cross plane of the lobed jet mixing flow.

to become more turbulent than that in the $Z/D=0.5$ ($Z/H=1.33$) cross plane. However, the ''signature'' of the lobed nozzle can still be identified from the instantaneous velocity field. The core jet flow was found to diffuse to the ambient flow substantially, and the size of the high-speed region in the center of the jet flow became smaller compared with that in the $Z/D=0.5$ ($Z/H=1.33$) cross plane given in the Fig. 5. The maximum value of the ensemble-averaged cross-stream velocity in the $X-Y$ plane is found to decrease to 4.3 m/s. Since the present lobed jet mixing flow is a free jet, the vector plot of the cross stream flow [Fig. 6(d)] shows that the center of the streamwise vortices have spread outward as they travel downstream. The same phenomena were also found in the LDV measurement results of Bleovich and Samimy.[18]

As the downstream distance increases to $Z/D=2.0$ ($Z/H=5.33$) (Fig. 7), the lobed jet mixing was found to become much more turbulent. The ''six-lobe structures'' of the core jet flow are nearly indistinguishable in the instantaneous velocity field. Although seven humps still can be found in the ensemble-averaged velocity field, which represent the high speed flow from the nozzle core and six lobes, they have become much more rounded than that in the upstream cross planes. The cross stream velocity vector shown on Fig. 7(d) also indicated that the magnitudes of the cross stream velocity have decreased quite a lot compared with those in upstream cross planes. The size of the high-speed region in the center of the jet flow and six lobes were found to decrease substantially due the intensive mixing of the core jet flow with ambient flow.

When the downstream distance increases to $Z/D=3.0$ ($Z/H=8.0$) (Fig. 8), the lobed jet mixing flow became so turbulent that the ''six-lobe structure'' of the core jet flow can not be identified in the instantaneous velocity field. The flow field is almost fully filled with many small-scale vortices. The ensemble-averaged velocity distribution also showed that the distinct hump representing the high-speed core jet flow has dissipated so seriously that the iso-velocity

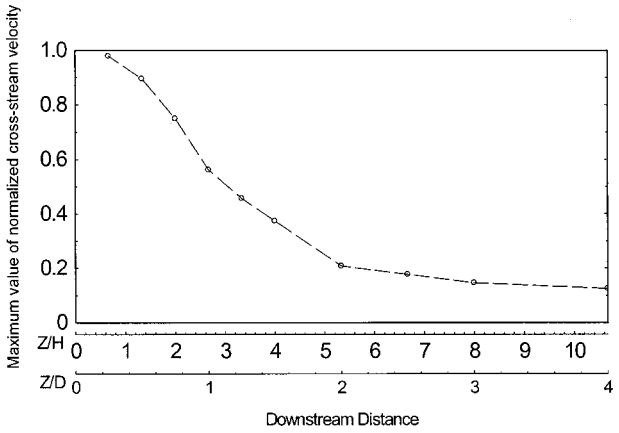

FIG. 9. Decay of the normalized maximum velocity of the ensemble-averaged cross stream in the lobed mixing flow.

contours of the high-speed core jet flow have become small concentric circles in the center of the jet flow. The ensemble-averaged cross stream velocity in this cross plane is so weak that it almost cannot be identified from the velocity vector plot.

Figure 9 shows the decay of the maximum value of the ensemble-averaged cross-stream velocity normalized by the value of $U_0 \cdot \sin(\theta_{\text{out}})$ with increasing downstream distance. It can be seen that the maximum velocity of the ensemble-averaged cross stream velocity decayed very quickly within the first two diameters due to intensive mixing of the core jet flow with ambient flow, then the decay rate became more moderate further downstream. In the downstream cross plane of $Z/D=2.0$ $(Z/H=5.33)$, the maximum value of the ensemble-averaged cross stream velocity became less than 20% of the value at the exit of the lobed nozzle.

Figure 10 shows the ensemble-averaged velocity fields in the circular jet flow at the same four cross planes as those shown in Figs. 5–8 for the lobed jet mixing flow. From the figures it can be seen that the ensemble-averaged velocity distribution of the circular jet was found to be a round hump as it is expected. As the downstream distance increases, the hump expands radially due to the growth of the shear layer between the core jet flow and ambient flow.

The streamwise vorticity distributions in the lobed jet mixing flow

The above velocity vector plots show the existence of a very strong cross stream (streamwise vortices) in the lobed jet mixing flow. The core jet flow expands outward along the lobes and ambient flow injects inward in the lobe troughs, which results in the generation of large-scale streamwise vortices with the vortex size on the order of the lobe height. A pair of counter-rotating streamwise vortices in the lobed jet mixing flow can be generated for each lobe. In order to study the evolution characteristics of these streamwise vortices quantitatively, the streamwise vorticity distributions in several cross planes of the lobed jet mixing flow were calculated based on the velocity data obtained by the stereoscopic PIV measurement. The normalized instantaneous streamwise vorticity (ϖ_z) and ensemble-averaged streamwise vorticity ($\overline{\varpi_z}$) were calculated based on the following equations:

$$\varpi_z = \frac{D}{U_0}\left(\frac{\partial v}{\partial x} - \frac{\partial u}{\partial y}\right), \tag{1}$$

$$\overline{\varpi_z} = \frac{D}{U_0}\left(\frac{\partial \overline{V}}{\partial x} - \frac{\partial \overline{U}}{\partial y}\right), \tag{2}$$

where the $D=40$ mm is the equivalent diameter of the test nozzle, $U_0=20$ m/s is the velocity of the core jet at the nozzle exit.

Figure 11(a) shows the instantaneous streamwise vorticity distribution in the $Z/D=0.5$ $(Z/H=1.33)$ cross plane. As indicated in the above velocity vector plots, six pairs of counter-rotating streamwise vortices were found to be generated in the lobed jet flow downstream of the six lobes. The size of these streamwise vortices is found to be equivalent to the height of the lobes. Compared with the instantaneous streamwise vorticity field, the ensemble-averaged streamwise vorticity was found to be smoother. The maximum value of the ensemble-averaged streamwise vorticity, which is about 4.0, is found to be a bit smaller than that of its instantaneous counterpart, which is about 4.5.

In the $Z/D=1.0$ $(Z/H=2.67)$ cross plane, the six pairs of the large-scale streamwise vortices shown in Fig. 11(a) were found to deform seriously. Some of the streamwise vortices were even found to break into smaller vortices [Fig. 12(a)]. The adjunct streamwise vortices were found to merge with each other to form a vortex ring in the lobe troughs, which is quite similar to the planar LIF flow visualization images shown in Fig. 4(d). The maximum value of the instantaneous streamwise vorticity in this cross plane was found to be almost at the same level as the value in the $Z/D=0.5$ $(Z/H=1.33)$ cross plane. From the ensemble-averaged streamwise vorticity distributions shown in Fig. 12(b), the six pairs of large-scale streamwise vortices were found to grow and expand radially. The strength of these ensemble-averaged streamwise vortices were found to decrease with the maximum value of the ensemble-averaged streamwise vorticity being about the half of that at the $Z/D=0.5$ $(Z/H=1.33)$ cross plane.

Besides the six pairs of large-scale streamwise vortices corresponding to the six lobes, six pairs of smaller and weaker streamwise vortices can also be identified from the ensemble-averaged streamwise vorticity distributions, which are at the six-lobe troughs. These smaller and weaker streamwise vortices at lobe troughs are the horseshoe vortex structures noted by Paterson,[10] which had also been visualized clearly in Fig. 4. McCormick and Bennett[14] also proved the existence of such horseshoe vortex structures in a planar lobed mixing flow.

As the downstream distance increased to $Z/D=2.0$ $(Z/H=5.33)$, the six pairs of large-scale streamwise vortices could no longer be easily identified from the instantaneous streamwise vorticity field shown in Fig. 13(a). Instead of large-scale streamwise vortices, many smaller streamwise vortices were found in the instantaneous streamwise vorticity

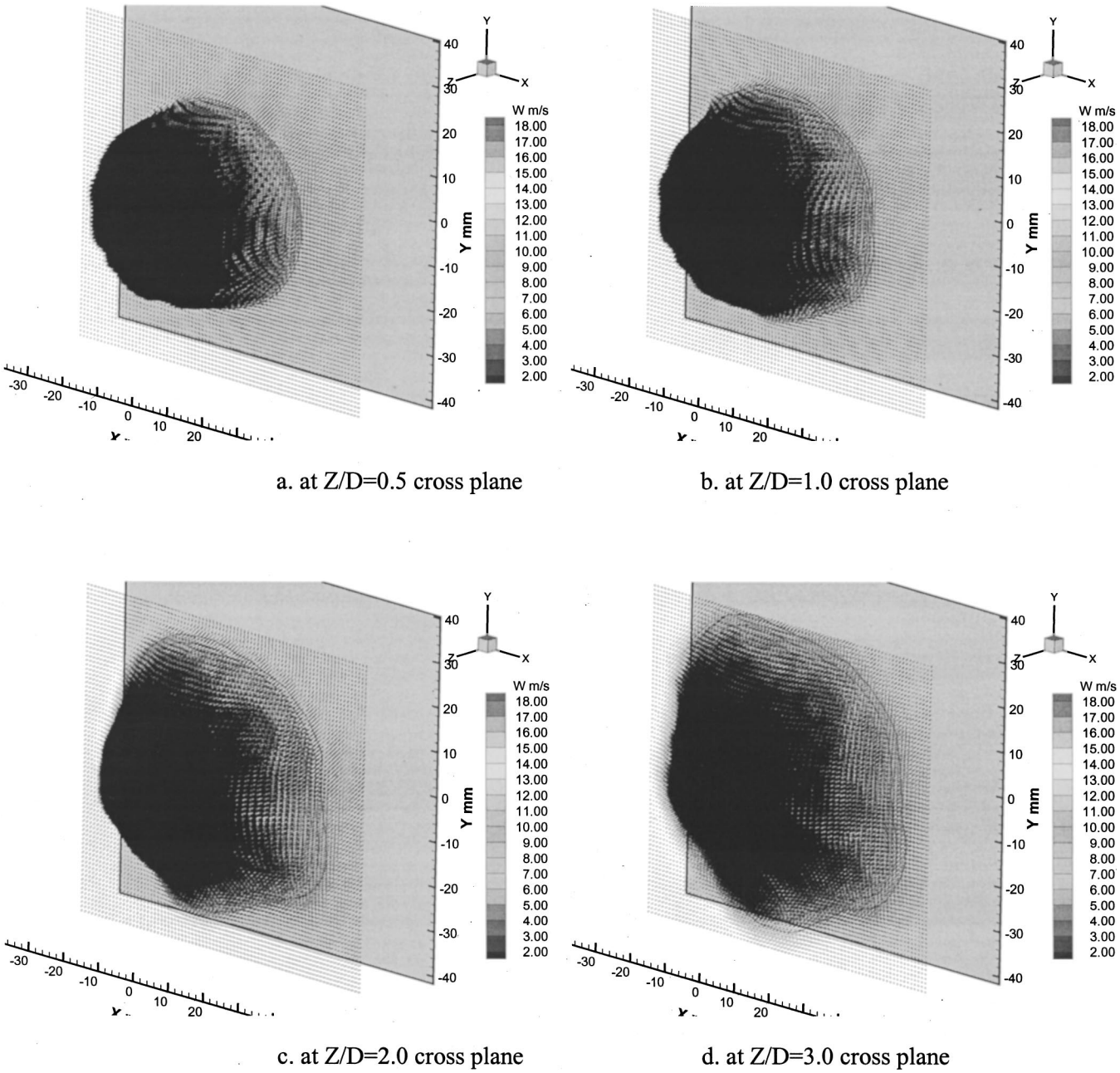

FIG. 10. The ensemble-averaged velocity fields in the circular jet flow.

distributions. The large-scale streamwise vortices observed in the upstream cross planes have been broken down into many smaller streamwise vortices. However, it should be mentioned that the maximum value of the instantaneous streamwise vorticity is found to be at the same level as those in the upstream cross planes.

From the ensemble-averaged streamwise vorticity distribution shown in Fig. 13(b), it can be seen that the large-scale streamwise vortices revealed in the ensemble-averaged streamwise vorticity distributions of upstream cross planes were found to break down into many smaller vortices. The strength of these streamwise vortices decayed substantially, and the maximum value of the ensemble-averaged streamwise vorticity was found to be just about one-fifth of that in the $Z/D=0.5$ ($Z/H=1.33$) cross plane.

As the downstream distance increased to $Z/D=3.0$ ($Z/H=8.0$) (Fig. 14), so many small-scale streamwise vortices were found to appear in the lobed jet mixing flow that they almost fully filled the measurement window. The maximum vorticity value of these smaller instantaneous streamwise vortices was found to be still at the same level of those in upstream cross planes. However, from the ensemble-averaged streamwise vorticty distribution in this cross plane, it can be seen that the size and strength of the ensemble-averaged steamwise vortices decreased substantially. The ''signature'' of the lobed geometry of the nozzle almost cannot be identified from the ensemble-averaged streamwise vorticity distribution.

From the above instantaneous streamwise distributions in different downstream cross planes, it can be seen that as

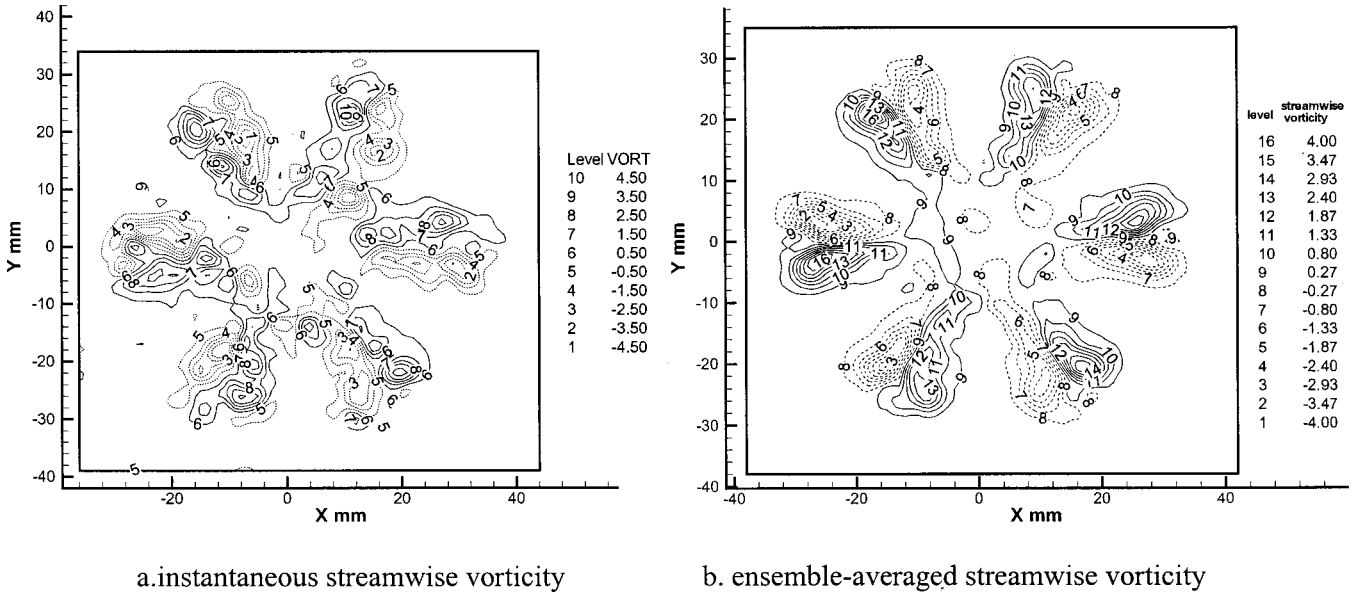

FIG. 11. The streamwise vorticity distributions at $Z/D=0.5$ ($Z/H=1.33$) cross plane of the lobed jet mixing flow.

the downstream distance increases, the size of the instantaneous streamwise vortices in the lobed jet mixing flow decreases. This indicates the large-scale streamwise vorticity generated by the lobed nozzle broke into smaller vortices as they travel downstream. However, the maximum vorticity values of the smaller vortices were found to be almost at the same level as their parent streamwise vortices. These results suggested that the dissipation of the large-scale streamwise vortices generated by the corrugated trailing edge of the lobed nozzle did not happen abruptly, but rather appeared to be a gradual process. The large streamwise vortices were found to break down into many smaller, but not weaker, streamwise vortices as the downstream distance increased. Thus, besides the mixing enhancement at large scale, mixing at a finer scale could also be achieved in the lobed jet mixing flow. The result, therefore, agrees well with those obtained by Belovich *et al.*[31]

The ensemble-averaged streamwise vorticity distribution can be used to indicate the overall effect of the special geometry of the lobed nozzle on the mixing processes in the lobed jet mixing flows. The cross stream generated by the special geometry of the lobed nozzle results in the generation of large-scale ensemble-averaged streamwise vortices in the lobed jet mixing flow. The large-scale ensemble-averaged streamwise vortices revealed in the ensemble-averaged streamwise vorticity distributions were found to grow up and expand radically within the first diameter, which may correspond to the streamwise vortex formation and intensification

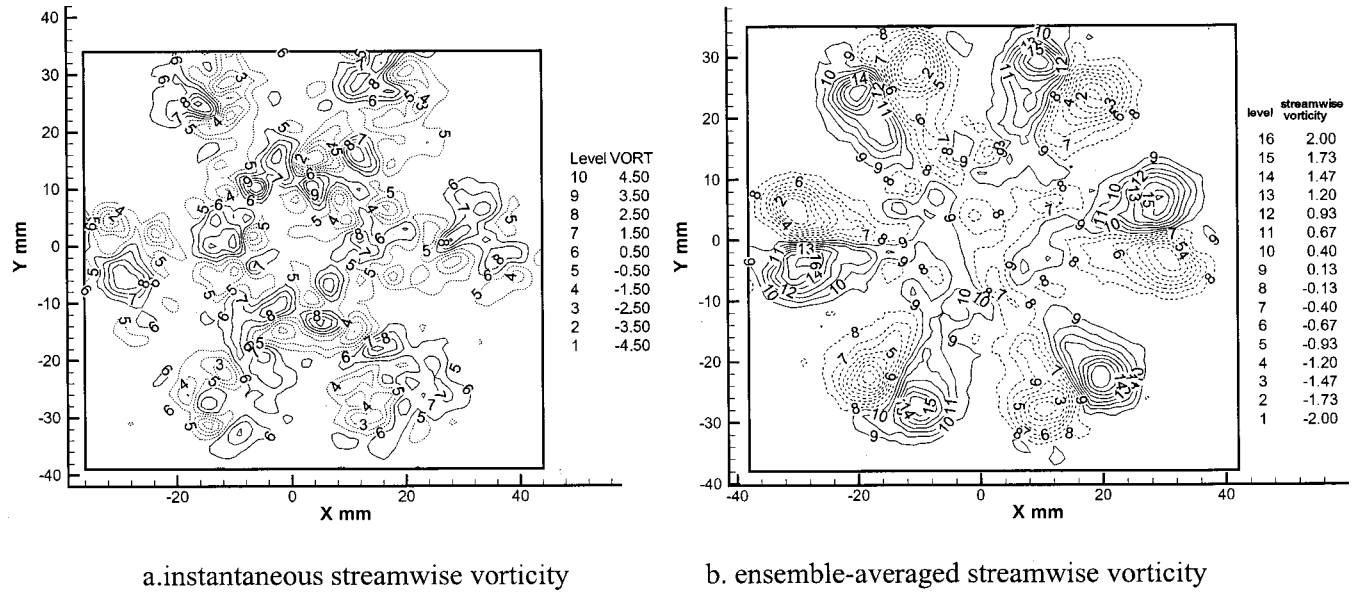

FIG. 12. The streamwise vorticity distributions at $Z/D=1.0$ ($Z/H=2.67$) cross plane of the lobed jet mixing flow.

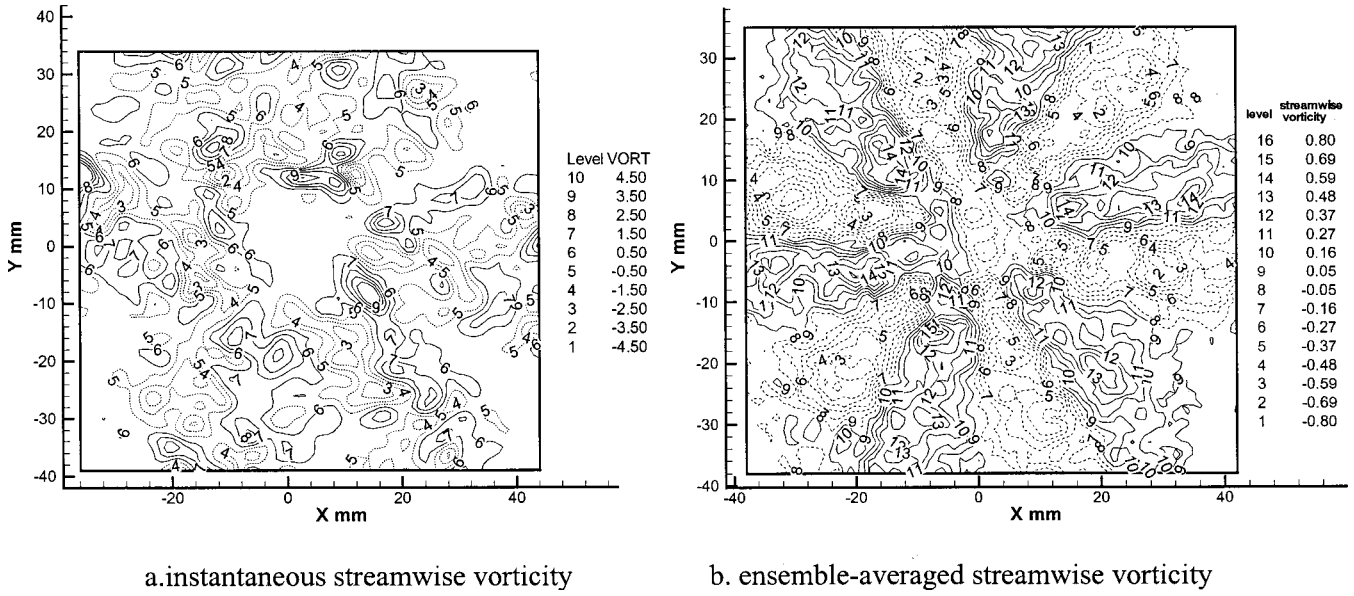

FIG. 13. The streamwise vorticity distributions at $Z/D=2.0$ ($Z/H=5.33$) cross plane of the lobed jet mixing flow.

steps suggested by Werle *et al.*[11] and Eckerle *et al.*[12] (Their LDV measurement results only reveal the ensemble-averaged streamwise vortices in a planar lobed mixing flow.) In the downstream cross planes of $Z/D=2.0$ (Fig. 13) and $Z/D=3.0$ (Fig. 14), the large-scale ensemble-averaged streamwise vortices were found to break down into smaller vortices. The strength of the ensemble-averaged streamwise vorticity was also found to decay rapidly as the downstream distance increases. Figure 15 gives the decay of the maximum value of the ensemble-averaged streamwise vorticity in the lobed jet flow quantitatively. From the figure, it can be seen that over the first diameter of the test nozzle, the ensemble-averaged streamwise vorticity decayed very rapidly. In the downstream region of the $Z/D=1.0$ ($Z/H=2.67$) cross plane, the large-scale ensemble-averaged streamwise vortices were found to break down into many smaller vortices, then the decay rate of the ensemble-averaged streamwise vorticity slows down. In the downstream cross plane of $Z/D=3.0$ ($Z/H=8.0$), the ensemble-averaged streamwise vorticity dissipated so seriously that the strength of the streamwise vortices became about one-tenth of that at the lobed nozzle exit. This may also indicate that the overall effect of the special geometry of the lobed nozzle on the jet flow mixing has almost disappeared at this downstream location. It should be noted that the profiles shown in Fig. 9 and in Fig. 15 are very similar. This may be explained by that since the streamwise vorticity is computed by taking the gradient of the cross-stream velocity components, therefore, the decay of ensemble-averaged streamwise vorticity

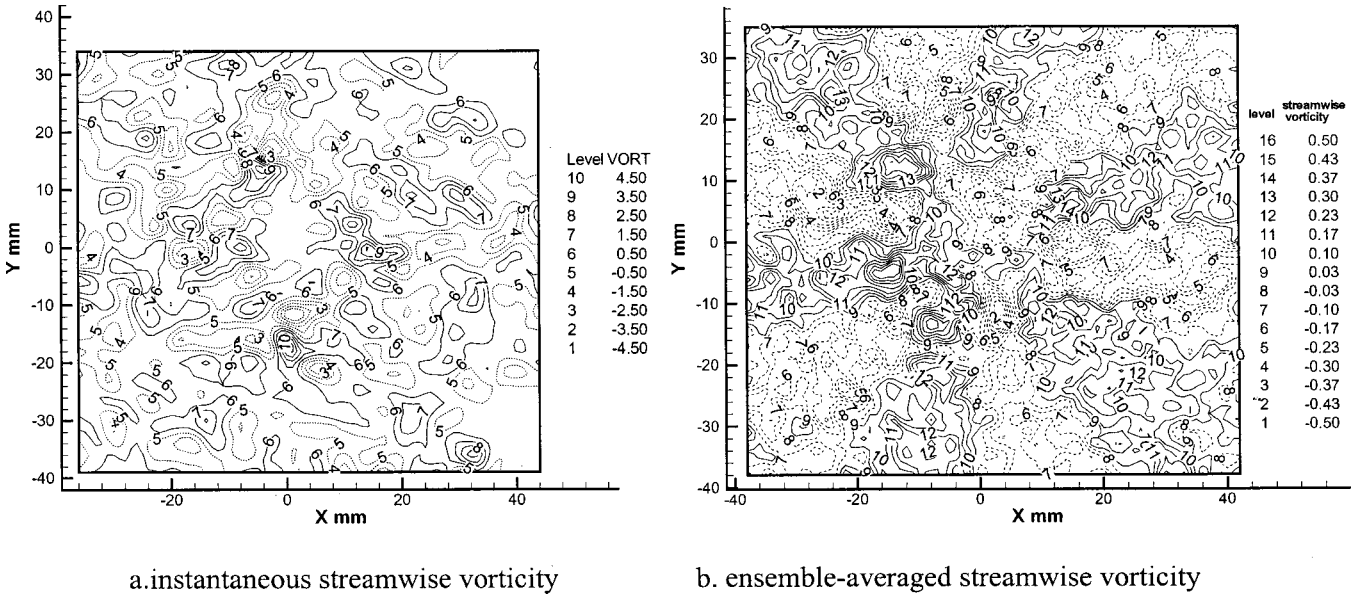

FIG. 14. The streamwise vorticity distributions at $Z/D=3.0$ ($Z/H=8.0$) cross plane of the lobed jet mixing flow.

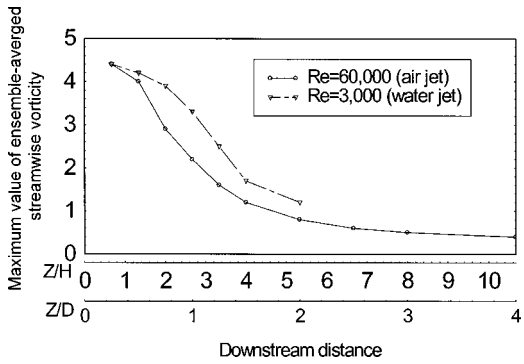

FIG. 15. The decay of the maximum value of the ensemble-averaged streamwise vorticity in the lobed jet mixing flow.

shown in Fig. 15 is quite similar to the decay of the maximum cross-stream velocity shown in Fig. 9.

Measurements of the same lobed nozzle at lower Reynolds numbers (water jet) using a conventional two-dimensional PIV system[19] is also given in Fig. 15. From the comparison of the maximum ensemble-averaged streamwise vorticity decay profiles at two Reynolds number levels, it can be seen that the ensemble-averaged streamwise vorticity at higher Reynolds numbers decayed more rapidly. This indicates that the location where the large-scale ensemble-averaged streamwise vortices break down into smaller vortices is expected to move upstream for the higher Reynolds number case.

The distribution of the turbulent kinetic energy

The mixing process between the core jet flow and ambient flow can be represented directly and quantitatively from the distribution of the turbulent kinetic energy distributions. The turbulent kinetic energy distributions of the lobed jet mixing flow in four selected cross planes are shown in Fig. 16. The turbulent kinetic energy values shown in these figures are calculated by using the following equation:

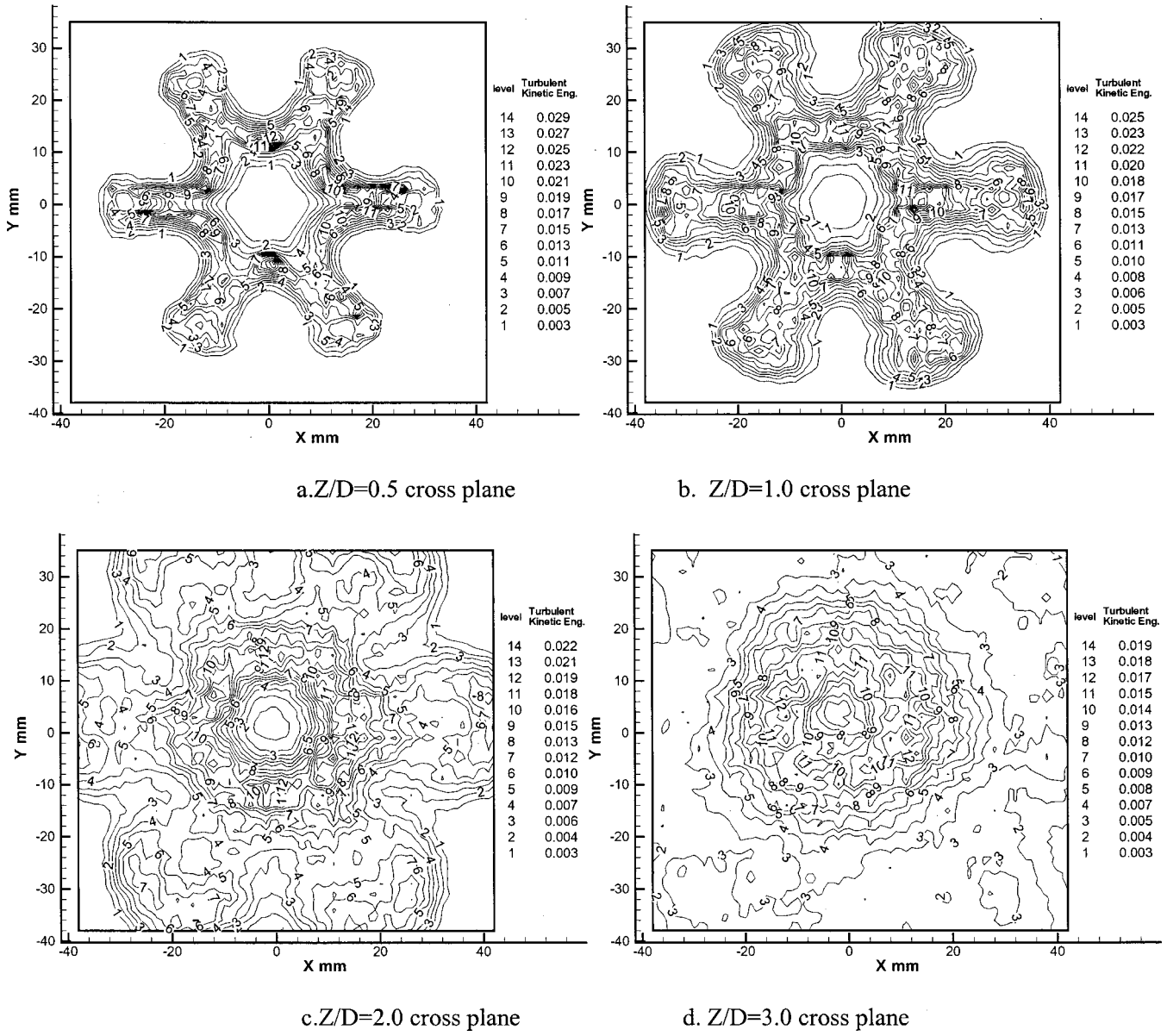

FIG. 16. The turbulent kinetic energy distributions in the lobed jet mixing flow.

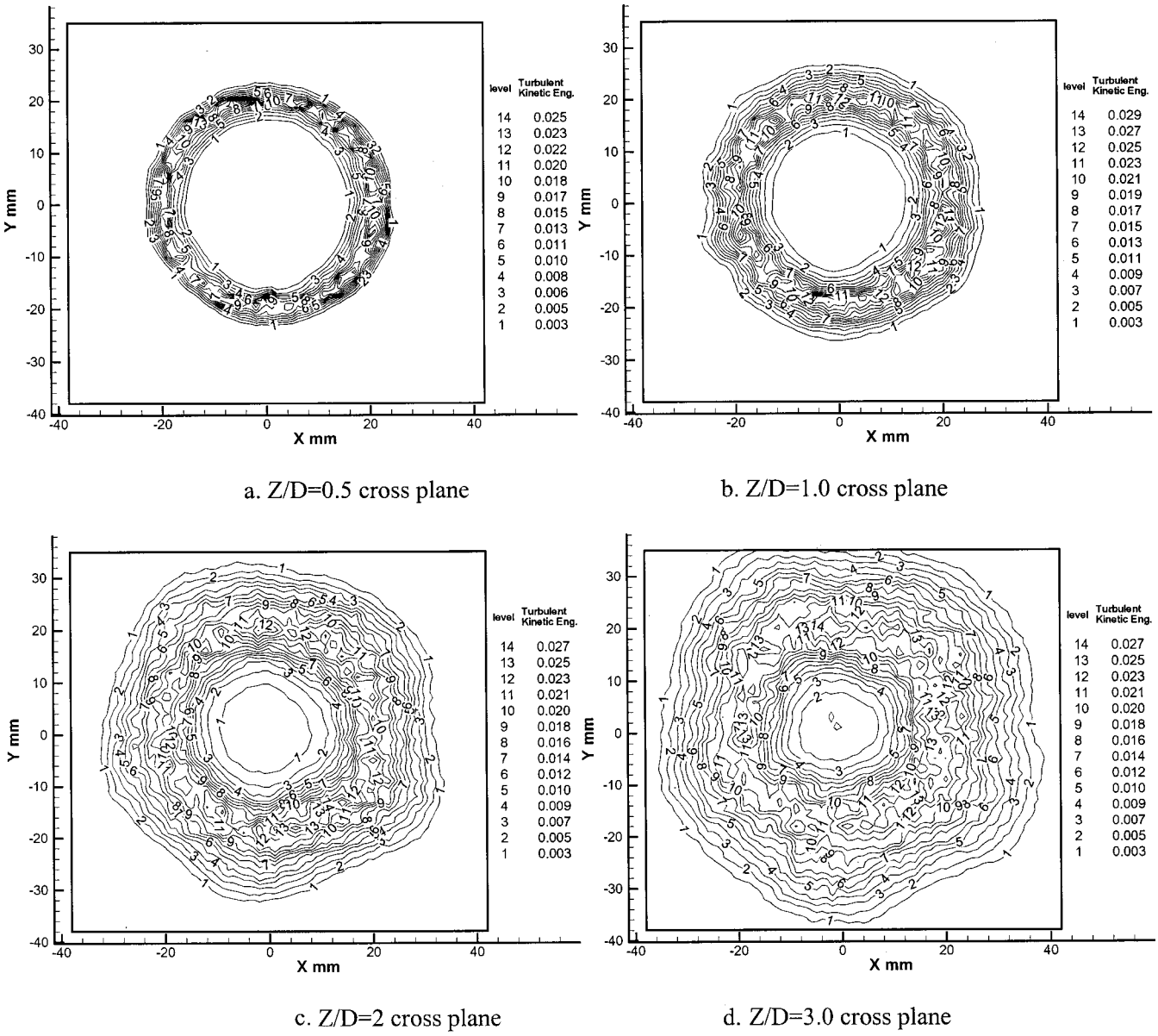

FIG. 17. The turbulent kinetic energy distributions in the circular jet flow.

$$K(x,y,z)=\frac{1}{2U_0^2}(\mathrm{rms}(u'))^2+(\mathrm{rms}(v'))^2+(\mathrm{rms}(w')^2)$$
$$=\frac{1}{2U_0^2}\left(\frac{1}{N}\sum_{t=1}^{N}(u_t-\overline{U})^2+\frac{1}{N}\sum_{t=1}^{N}(v_t-\overline{V})^2+\frac{1}{N}\sum_{t=1}^{N}(w_t-\overline{W})^2\right), \quad (3)$$

where $N=400$ is the number of the instantaneous stereoscopic PIV measurement frames used for the ensemble-averaged parameter calculation. u_t, v_t, and w_t are the instantaneous velocity components in x, y, and z direction, while $\overline{U}$, $\overline{V}$, and $\overline{W}$ are the ensemble-averaged velocity components.

In the $Z/D=0.5$ ($Z/H=1.33$) cross plane, the contour of the turbulent kinetic energy distribution was found to exhibit the lobed nozzle "signature," which indicates that mixing of the core jet flow with ambient flow is conducted mainly at the interface of the two streams. A low turbulent kinetic energy region was found in the center, which corresponds to the unmixed high-speed core in the center of the jet flow. It should also be noted that the regions with higher turbulent kinetic energy values are found to concentrate at the lobe troughs instead of lobe peaks. This may be caused by the earlier rolling-up of the azimuthal Kelvin–Helmholtz vortices at the lobed troughs, which has been reported and visualized in the earlier work of the authors[19] by using planar laser induced fluorescence (LIF) technique.

In the $Z/D=1.0$ ($Z/D=2.67$) cross plane, the mixing area between the core jet flow and ambient flow was found to increase and the mixing region was found to expand outward and inward. The unmixed core jet flow in the center of the jet flow decreased. The contour of the turbulent kinetic energy distribution was found to form "mushrooms structures" in the downstream projections of the lobed peaks, which may

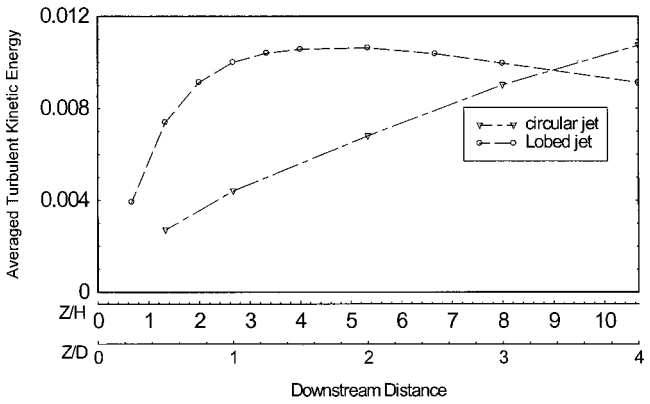

FIG. 18. The averaged turbulent kinetic energy profile in the lobed jet mixing flow and the circular jet flow.

be caused by the pinch-off effect of the streamwise vortices on the azimuthal Kelvin–Helmholtz vortices suggested by McCormick and Bennett.[14] The similar ''mushrooms structures'' in the lobed jet flow has also been reported by Belovich *et al.*[31] in their passive scalar measurement results.

As the downstream distance increased to $Z/D=2.0$ ($Z/H=5.33$), the mixing region between the core jet flow and ambient flow increased substantially, which almost filled the investigation window fully. The adjacent ''mushroom structures'' merged with each other. At the $Z/D=3.0$ ($Z/H=8.0$) cross plane, the contour of the turbulent kinetic energy were found to be circular, which is quite similar to that in the far field of a circular jet flow.

Figure 17 shows the turbulent kinetic energy distributions in the same cross planes for the circular jet flow. At the exit of the circular jet flow, the contour of the turbulent kinetic energy distribution was found to be a thin ''ring structure'' as it is expected. As the downstream distance increased, the ''ring structure'' was found to expand inward and outward, which corresponds to the growth of the shear layer between the core jet flow and ambient flow. Compared with the turbulent kinetic energy distribution in the lobed jet mixing flow at the same downstream locations, it can be seen that the area of the mixing region in the lobed jet mixing flow will be much bigger than that in the circular jet.

In order to compare the mixing effectiveness in the lobed jet mixing flow and circular jet flow more clearly and quantitatively, averaged turbulent kinetic energy (ATKE) of the jet mixing flows (Fig. 18) at each measured cross plane were calculated by using the following equation:

$$\mathrm{ATKE}=\frac{\int \rho \overline{W}(x,y,z)K(x,y,z)dx\,dy}{\int \rho \overline{W}(x,y,z)dx\,dy}, \tag{4}$$

where ρ is density of the air jet flows, $\overline{W}$ is the ensemble-averaged velocity in the Z-direction and K is the turbulent kinetic energy value of the stereoscopic PIV measurement result at each measurement cross plane.

For the lobed jet mixing flow, it can be seen that the averaged turbulent kinetic energy profile grew very rapidly within first diameter of the test nozzle, then decrease to a more moderate rate in the downstream region of $Z/D>1.0$ ($Z/H>2.67$). The ATKE growth rate reached the peak value at $Z/D=2.0$ ($Z/H=5.33$), then began to decrease. This is because that within the first one diameter of the test nozzle ($Z/H<2.67$), due to the stirring effect of the large-scale streamwise vortices revealed in the ensemble-averaged streamwise vorticity distributions, the core jet flow and ambient flow mixed intensively. In the downstream region of $Z/D>1.0$ ($Z/H>2.67$), the large-scale streamwise vortices generated by the lobed nozzle were found to break down into smaller vortices, i.e., the stirring effect of the ensemble-averaged streamwise vortices weakened. So, the growth rate of the averaged turbulent kinetic energy was found to decrease, and reach its peak at the $Z/D=2.0$ ($Z/H=5.33$) cross plane. The ensemble-averaged streamwise vorticity has become so weak that it almost cannot affect the mixing process in the downstream region of $Z/D>2.0$ ($Z/H>5.33$). Most of the turbulent kinetic energy in the lobed jet mixing flow dissipated in the intensive mixing upstream, so the av-

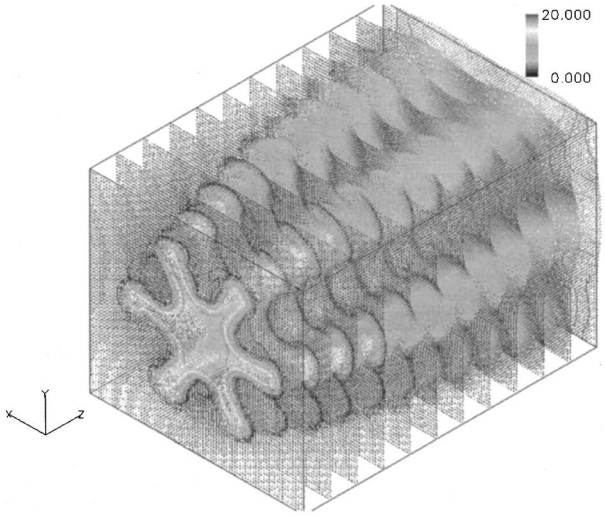

a. ensemble averaged velocity vectors

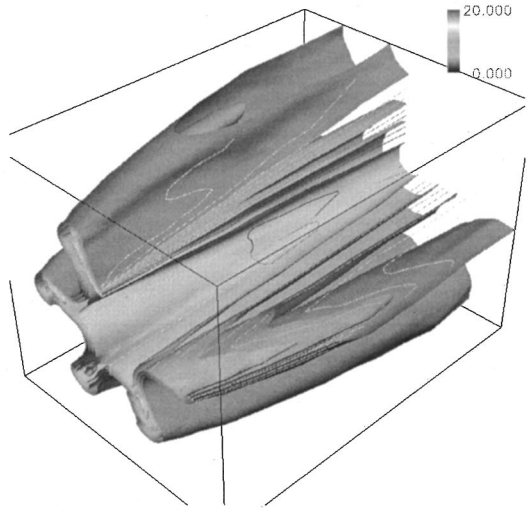

b. velocity iso-surfaces

FIG. 19. Reconstructed three-dimensional flow fields of the lobed jet mixing flow in the near region ($Z/D<3.0$).

eraged turbulent kinetic energy begins to decrease further downstream. It also indicates that most of the enhancement of mixing caused by the lobe nozzle occurs within the first two diameters. The mixing between the core jet flow and ambient flow beyond the first two diameters occurs by the same gradient-type mechanism as that for a conventional circular jet. This result is also found to agree with the findings of McCormick and Bennett[14] and Glauser *et al.*[17] in a planar lobed mixing flow, who suggested that the maximum effectiveness region for a lobed mixer is about the first six lobe heights.

For the circular jet flow, the averaged turbulent kinetic energy is found to grow linearly in the investigated region ($Z/D<4.0$). The linear growth behavior is consistent with classical thin-layer approximations assuming simple eddy-viscosity turbulent transport.[32] At the exit of the nozzle, the averaged turbulent kinetic energy in lobed jet mixing flow is found to be much greater than that in the circular jet flow. This is believed to be caused by the mixing enhancement associated with the increased initial interfacial area of the lobe geometry as suggested by Elliott *et al.*[13]

As mentioned above, the enhancement of mixing caused by the special geometry of the lobes is almost negligible after the first two diameters, and the mixing between the core jet flow and ambient flow will occur by the same gradient-type mechanism as that of a conventional circular jet flow. Due to the intensive mixing upstream, the velocity of the core jet flow decays very quickly. A weaker shear layer (lower velocity ratio) is expected in the further downstream region ($Z/D>3.0$ and $Z/H>8.0$) of the lobed jet mixing flow compared with circular jet flow. Therefore, in the further downstream region ($Z/D>3.0$, $Z/H>8.0$), the averaged turbulent kinetic energy of lobed jet mixing flow was found to be smaller than the circular jet flow. McCormick and Bennett[14] reported similar results in the far field of a planar lobed mixer flow field.

Reconstructed three-dimensional flow field

Based on the stereoscopic PIV measurement results at 12 cross planes of the lobed jet mixing flow, the three-dimensional flow field at the near field ($Z/D<3.0$) of the lobed jet mixing flow was reconstructed. Figure 19(a) shows the three-dimensional ensemble-averaged velocity vectors. The velocity iso-surfaces reconstructed from the three-dimensional measurement results are shown in Fig. 19(b). The velocity magnitudes of these iso-surfaces are 4 m/s, 8 m/s, 12 m/s, and 16 m/s, respectively. From the reconstructed three-dimensional velocity vectors and velocity iso-surfaces, the three-dimensional features of the lobed jet mixing flow can be seen clearly.

CONCLUSIONS

In the present study, the flow field in the first four diameters of a lobed jet mixing flow and a conventional circular jet flow were measured by using a high-resolution stereoscopic PIV system. The characteristics of the mixing process in the lobed jet mixing flow were compared with the conventional circular jet flow. The existence of large-scale streamwise vortices in the lobed jet mixing flow is revealed clearly from stereoscopic PIV measurements. From the instantaneous streamwise vorticity distributions of the lobed jet mixing flow, it can be seen that the large-scale streamwise vortices generated by the corrugated trailing edge of the lobed nozzle break into smaller, but not weaker streamwise vortices gradually as they travel downstream. This is proposed as the reason that a lobed nozzle can enhance both the large-scale mixing and small-scale mixing in flow field as reported in previous studies. The overall effect of the lobed nozzle on mixing process in the lobed jet flow was evaluated by analyzing the ensemble-averaged streamwise vorticity distributions. The ensemble-averaged streamwise vortices in the lobed jet flow were found to expand radially within the first diameter downstream, then break down into smaller and weaker vortices in the following region, as has been called as the formation, intensification, and breakdown processes by other researchers. The strength of the ensemble-averaged streamwise vorticity was found to decay very rapidly over the first diameter of the lobed nozzle, then decay at a more moderate rate further downstream. The turbulent kinetic energy distributions also indicated that most of the intensive mixing between the core jet flow and ambient flow occurred over the first two diameters of the lobed jet flow (first six lobe heights). In the downstream cross plane of three nozzle diameters, contours of turbulent kinetic energy distribution are quite similar to those in a circular jet flow at far field. These may indicate the mixing enhancement caused by the special geometry of the lobed nozzle is almost finished after the first two diameters downstream of the lobed nozzle (first six lobe heights). The mixing between the core jet flow and ambient flow further downstream of the lobed jet mixing flow will occur by the same gradient-type mechanism as that for a circular jet flow.

[1] K. B. M. Q. Zaman, "Axis switching and spreading of an asymmetric jet: The role of coherent structure dynamics," J. Fluid Mech. **316**, 1 (1997).
[2] A. P. Kuchar and R. Chamberlin, "Scale model performance test investigation of exhaust system mixers for an energy efficient engine (E^3)," AIAA Paper No. 80-0229, 1980.
[3] W. M. Presz, G. Reynolds, and D. McCormick, "Thrust augmentation using mixer-ejector-diffuser systems," AIAA Paper No. 94-0020, 1994.
[4] G. D. Power, M. D. McClure, and D. Vinh, "Advanced IR suppresser design using a combined CFD/Test approach," AIAA Paper No. 94-32l5, l994.
[5] H. Hu, T. Saga, T. Kobayashi, N. Taniguchi, H. Liu, and S. Wu, "Research on the rectangular lobed exhaust ejector/mixer systems," Trans. Jpn. Soc. Aeronautics Space Sci. **41**, 187 (1999).
[6] L. L. Smith, A. J. Majamak, I. T. Lam, O. Delabroy, A. R. Karagozian, F. E. Marble, and O. I. Smith, "Mixing enhancement in a lobed injector," Phys. Fluids **9**, 667 (l997).
[7] S. A. Skebe, D. C. McComich, and W. M. Presz, "Parameter effects on mixer-ejector pumping performance," AIAA Paper No. 88-0188, 1988.
[8] S. C. M. Yu, T. H. Yip, and C. Y. Liu, "Mixing characteristics of forced mixers with scalloped lobes," J. Propul. Power **13**, 305 (1997).
[9] W. M. Presz, R. Gousy, and B. Morin, "Forced mixer lobes in ejector designs," AIAA Paper No. 86-1614, 1986.
[10] R. W. Paterson, "Turbofan forced mixer nozzle flowfield—A benchmark experimental study," ASME J. Eng. Gas Turbines Power **106**, 692 (1984).
[11] M. J. Werle, R. W. Paterson, and W. M. Presz, "Flow structure in a periodic axial vortex array," AIAA Paper No. 87-6l0, 1987.
[12] W. A. Eckerle, H. Sheibani, and J. Awad, "Experimental measurement of the vortex development downstream of a lobed forced mixer," J. Eng. Gas Turbines Power **114**, 63 (1992).
[13] J. K Elliott, T. A. Manning, Y. J. Qiu, C. S. Greitzer, C. S. Tan, and T. G.

Tillman, ''Computational and experimental studies of flow in multi-lobed forced mixers,'' AIAA Paper No. 92-3568, 1992.
[14]D. C. McCormick and J. C. Bennett, ''Vortical and turbulent structure of a lobed mixer free shear layer,'' AIAA J. **32**, 1852 (l994).
[15]L. Ukeiley, M. Varghese, M. Glauser, and D. Valentine, ''Multifractal analysis of a lobed mixer flowfield utilizing the proper orthogonal decomposition,'' AIAA J. **30**, 1260 (1992).
[16]L. M. Ukeiley, M. Glauser, and D. Wick, ''Downstream evolution of POD eigenfunctions in a lobed mixer,'' AIAA J. **31**, 1392 (1993).
[17]M. Glauser, L. Ukeiley, and D. Wick, ''Investigation of turbulent flows via pseudo flow visualization, Part 2: The lobed mixer flow field,'' Exp. Therm. Fluid Sci. **13**, 167 (1996).
[18]V. M. Belovich and M. Samimy, ''Mixing process in a coaxial geometry with a central lobed mixing nozzle,'' AIAA J. **35**, 838 (l997).
[19]H. Hu, T. Saga, T. Kobayashi, and N. Taniguchi, ''Research on the vortical and turbulent structures in the lobed jet flow by using LIF and PIV,'' Meas. Sci. Technol. **11**, 698 (2000).
[20]A. K. Prasad and R. J. Adrian, ''Stereoscopic particle image velocimetry applied to fluid flows,'' Exp. Flows **15**, 49 (1993).
[21]A. Melling, ''Tracer particles and seeding for particle image velocimetry,'' Meas. Sci. Technol. **8**, 406 (1997).
[22]A. K. Prasad and K. Jensen, ''Scheimpflug stereocamera for particle image velocimetry in liquid flows,'' Appl. Opt. **34**, 7092 (1995).
[23]S. M. Soloff, R. J. Adrian, and Z. C. Liu, ''Distortion compensation for generalized stereoscopic particle image velocimetry,'' Meas. Sci. Technol. **8**, 1441 (1997).
[24]D. F. Hill, K. V. Sharp, and R. J. Adrian, ''Stereoscopic particle image velocimetry measurements the flow around a rushton turbine,'' Exp. Flows **29**, 478 (2000).
[25]A. K. Parsad, ''Stereoscopic particle image velocimetry,'' Exp. Fluids **29**, 103 (2000).
[26]Z. Watanabe, M. Natori, and Z. Okkuni, ''Fortran 77 Software for Numerical Computation,'' MARUZEN Publication, C3055, 1989 (in Japanese).
[27]H. Hu, T. Saga, T. Kobayashi, N. Taniguchi, and S. Segawa, ''The spatial resolution improvement of PIV result by using hierarchical recursive operation,'' Proceedings of 9th International Symposium on Flow Visualization, Edinburgh, Scotland, 22–25 August 2000.
[28]D. P. Hart, ''PIV error correction,'' Exp. Fluids **29**, 13 (2000).
[29]H. Hu, T. Saga, T. Kobayashi, N. Taniguchi, and K. Okamoto, ''Evaluation of the cross-correlation method by using PIV standard image,'' J. Visual. **1**, 87 (1998).
[30]H. Hu, ''Investigation on lobed jet mixing flows by using PIV and LIF techniques,'' Ph.D. thesis, The University of Tokyo, Tokyo, Japan, 2001.
[31]V. M. Belovich, M. Samimy, and M. F. Reeder, ''Dual stream axisymmetric mixing in the presence of axial vorticity,'' J. Propul. Power **12**, 178 (l996).
[32]H. Tennekes and J. L. Lumley, *A First Course in Turbulence* (MIT Press, Cambridge, MA, 1972).